12th International Symposium on Turbulence and Shear Flow Phenomena (TSFP12)
Osaka, Japan (Online), July 19-22, 2022

ULTIMATE HEAT TRANSFER IN TURBULENT THERMAL CONVECTION BETWEEN POROUS WALLS

Fanyu Meng
Graduate School of Engineering Science
Osaka University
1-3 Machikaneyama, Toyonaka,
Osaka 560-8531, Japan
meng@tes.me.es.osaka-u.ac.jp

Shingo Motoki
Graduate School of Engineering Science
Osaka University
1-3 Machikaneyama, Toyonaka,
Osaka 560-8531, Japan
motoki@me.es.osaka-u.ac.jp

Genta Kawahara
Graduate School of Engineering Science
Osaka University
1-3 Machikaneyama, Toyonaka,
Osaka 560-8531, Japan
kawahara@me.es.osaka-u.ac.jp

ABSTRACT

A numerical study on the heat transfer and flow structure has been conducted for turbulent thermal convection between horizontal porous walls by using the immersed boundary method. In this research, we perform direct numerical simulation with high-order compact schemes for turbulent Rayleigh-Bérnard(RB) convection at the Rayleigh number $Ra = 4 \times 10^8$–8×10^8. The ultimate state represented by the scaling $Nu \sim Ra^{1/2}$ for this RB convection between porous walls could be well achieved at a high Rayleigh number Ra, where the appearance of the large-scale structures within the near-wall region hold the existence of the ultimate state. Moreover, a transient state without a power law of Nu with Ra with an distinct exceeded ultimate scaling $Nu \sim Ra$ could also be observed at the lower Ra. The distinct increased vertical velocity over the terminal velocity has been recognized as the trigger of this novel scaling-like transitional process. The mechanism of transition to the ultimate state has been well investigated and discussed based on the energy dissipation rate and vortical structures in this research.

Introduction

Rayleigh-Bénard (RB) convection is a canonical thermal flow system induced by buoyancy in horizontal fluid layer heated from below and cooled from above. The key parameters of this flow system are the Rayleigh number and the Prandtl number, defined as $Ra = g\alpha\Delta TH^3/(\nu\kappa)$ and $Pr = \nu/\kappa$, where g, α, κ and ν represent the acceleration of gravity, expansion coefficient, thermal diffusion coefficient and viscosity, respectively. The Rayleigh number Ra expresses the strength of buoyancy caused by gravity and temperature difference. The Nusselt number Nu is defined to evaluate the intensity of a heat flux in comparison to thermal conduction. A power law $Nu \sim Ra^{\gamma}$ has been long discussed, in which different values of γ demonstrate distinct states in this system. Malkus (1954) and Priestley (1954) derived an $Nu \sim Ra^{1/3}$ law with a marginal instability analysis and similarity argument, respectively. In contrast, Kraichnan (1962) predicted an asymptotic ultimate regime as $Nu \sim Pr^{1/2}Ra^{1/2}$ with a logarithm correction stemming from turbulent boundary layers. The most notable implication is that the heat transport will be independent of thermal conductivity or thermal diffusivity in the ultimate state. Several attempts had been done to achieve the ultimate scaling by Calzavarini *et al.* (2005) , Pawar & Arakeri (2016) and Zhu *et al.* (2019) numerically and experimentally.

According to previous studies, the effects induced by the wall has been recognized to prevent heat transfer thereon from exhibiting the ultimate scaling. With the aid of wall permeability first introduced by Jiménez *et al.* (2001), Kawano *et al.* (2021) showed that the ultimate scaling can be well realized at high Rayleigh number in turbulent thermal convection between Darcy-type permeable walls on which the vertical velocity is given by $w = \pm\beta p/\rho$. On the porous walls of fixed geometry, the dimensionless permeability parameter βU_f (U_f being the buoyancy-induced terminal velocity) is considered to increase as $\beta U_f \sim Pr^{-1/2}Ra^{1/2}$ with increasing Ra, and thus in a real situation the prefactor c in the scaling law $Nu = cRa^{\gamma}$ increases with increasing Ra, implying deviation from the power law, i.e. the ultimate scaling of $\gamma = 1/2$. To achieve the ultimate scaling and verify the deviation from the ultimate scaling in a more realistic model for the RB convection, we performed direct numerical simulations based on high-order compact schemes and implemented the immersed boundary method to mimic the interaction to let it be more realistic and realizable.

Governing equations and flow configuration

A staggered finite-difference code Incompact3D developed by Laizet & Lamballais (2009) and Laizet & Li (2011) based on high-order compact schemes has been applied to ensure a quasi-spectral accuracy. The immersed boundary method was used to make the detailed effects induced by the

geometry structures in this flow system. The Boussinesq equations, which employs the Oberbeck-Boussinesq approximation in the Navier-Stokes equation are our governing equations,

$$\frac{\partial \boldsymbol{u}}{\partial t} + (\boldsymbol{u}\cdot\nabla)\boldsymbol{u} = -\frac{1}{\rho}\nabla p + \nu\nabla^2\boldsymbol{u} + g\alpha T\boldsymbol{e}_z + \boldsymbol{f}_b \tag{1}$$

$$\nabla\cdot\boldsymbol{u} = 0 \tag{2}$$

$$\frac{\partial T}{\partial t} + (\boldsymbol{u}\cdot\nabla)T = \kappa\nabla^2 T + q_b \tag{3}$$

in which, $\boldsymbol{u}(\boldsymbol{x},t) = u\boldsymbol{e}_x + v\boldsymbol{e}_y + w\boldsymbol{e}_z$ and $T(\boldsymbol{x},t)$ denote the velocity field and temperature field respectively. The velocity field and temperature field in this case follow the periodic boundary conditions in the horizontal x- and y-directions with the same length as $L_x = L_y = H$. The $\boldsymbol{f}_b$ and q_b denote the force field and heat source term on account of the implemented immersed boundary method, respectively. We use the buoyancy-induced terminal velocity, $U_f = (g\alpha\Delta TH)^{1/2}$ as a reference velocity scale. Pr and Ra are control parameters in the system and the Pr is set to unity in this study. Moreover, the aspect ratio i.e., the ratio of the horizontal extent to the height is also a control parameter. The boundary conditions for computational domain of liquid parts have been set as blow,

$$u(z=0) = u(z=3H) = w(z=0) = w(z=3H) = 0 \tag{4}$$

$$T(z=0) = T(z=3H) = 0 \tag{5}$$

and the boundary conditions for the solid parts are imposed as no-slip and isothermal,

$$u = v = w = 0 \tag{6}$$

$$T(z < H|_{solid}) = \Delta T \tag{7}$$

$$T(z > 2H|_{solid}) = 0 \tag{8}$$

The intensity of the convection will be quantified in terms of the heat flux resulting from the temperature difference between the top and bottom walls given by Nusselt number Nu,

$$Nu = \frac{-\kappa\frac{\mathrm{d}\langle T\rangle_{xyt}}{\mathrm{d}z} + \langle wT\rangle_{xyt}}{\kappa\Delta T/H} \tag{9}$$

where $<\cdot>_{xyt}$ denotes the horizontal and time average on the variables at the center of domain.

The geometry and flow configuration are shown in Figure 1. The porous wall possesses a 10×10 matrix of square holes.

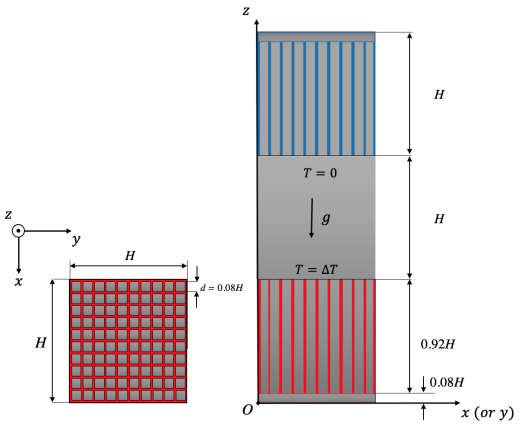

Figure 1: The geometry of porous patterns and flow configurations for simulations. The left slice shows the holes in porous media viewed from above. The right one shows all the flow system viewed from the side. The red part, blue part and grey part denote the heating porous wall, cooling porous wall and fluid domain, respectively.

The temperature of the heated lower (or cooled upper) porous wall is kept at $T = \Delta T > 0$ (or $T = 0$). The boundary conditions of the surfaces on the porous media and the two base plates at $z = 0$ and $z = 3$H overhead and underneath are no-slip and isothermal. The width of square holes is set to 0.08H in all simulations. There are plenum chambers of height 0.08H between the porous media and the base plates. The chamber is an an important part in this simulation, which make the fluid get in and get out from the porous walls be more realizable. Moreover, according to several previous studies, the permeable wall without chamber can be considered as the roughness.

Scaling properties

The scaling relationship not only between the Ra and Nu but also the statistical features of vertical velocity induced by buoyancy term and temperature distributions will be studied and considered. It can be easily observed from Figure 2, that the ultimate scaling $Nu \sim Ra^{1/2}$ is achieved by the introduction of the porous walls with chambers at the high Rayleigh number $Ra > 10^8$. The observed ultimate scaling in the case of the porous walls is roughly consistent with that found by Kawano *et al.* (2021). in the case of the permeable walls at $\beta U_f = 3$. At the lower Rayleigh number $Ra < 10^8$ in the case of porous walls, a distinct scaling law which almost dominated all the transition process can be observed, $Nu \sim Ra$. This kind of scaling law exceeded the ultimate scaling and enhanced the Nu intensely, so it can be called as a scaling-like transition process and this process is so novel when considered about several studies. At the much lower Rayleigh number around $Ra = 10^6$, Nu in the conventional non-porous case is almost comparable with that in the porous case, implying that the wall porosity does not have significant effects on thermal convection.

From Figure 3, the relationship between the Ra and Nu on different positions can be observed. Most notable thing is that, as $Ra > 10^8$ the ultimate state is reached in almost every position of the domain. Likewise, the same scaling law $Nu \sim Ra$ is evident in every position of the domain when the global state is in this scaling-like transition state.

The mean profile of temperature distribution has been

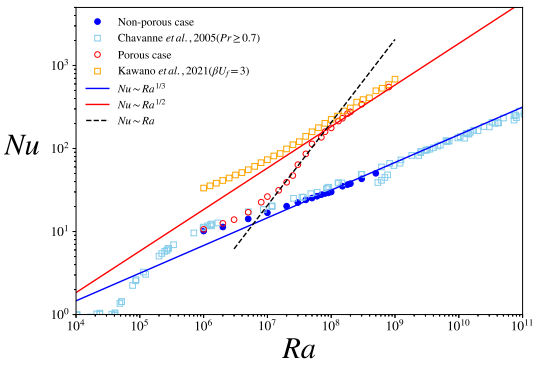

Figure 2: Nusselt number Nu as a function of Rayleigh number Ra. The blue line and red lines represent the classical scaling $Nu \sim Ra^{1/3}$ and the ultimate scaling $Nu \sim Ra^{1/2}$ respectively. The black dashed line denotes the distinct scaling-like transition process with scaling law $Nu \sim Ra$. The blue circles represent the results obtained from the non-porous RB convection and the sky-blue squares denote the experimental data in a non-porous cylindrical cell done by Chavanne *et al.* (2001). The red circles represent the results obtained from the RB convection between porous walls. The orange squares represent the results obtained from Kawano *et al.* (2021) for the RB between permeable walls at $\beta U_f = 3$

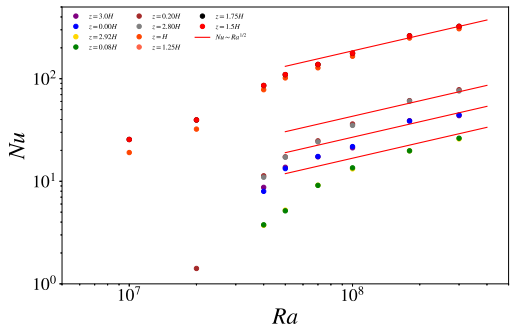

Figure 3: Nusselt number Nu as a function of Rayleigh number Ra for porous cases with different positions. The red line represents the ultimate scaling $Nu \sim Ra^{1/2}$.

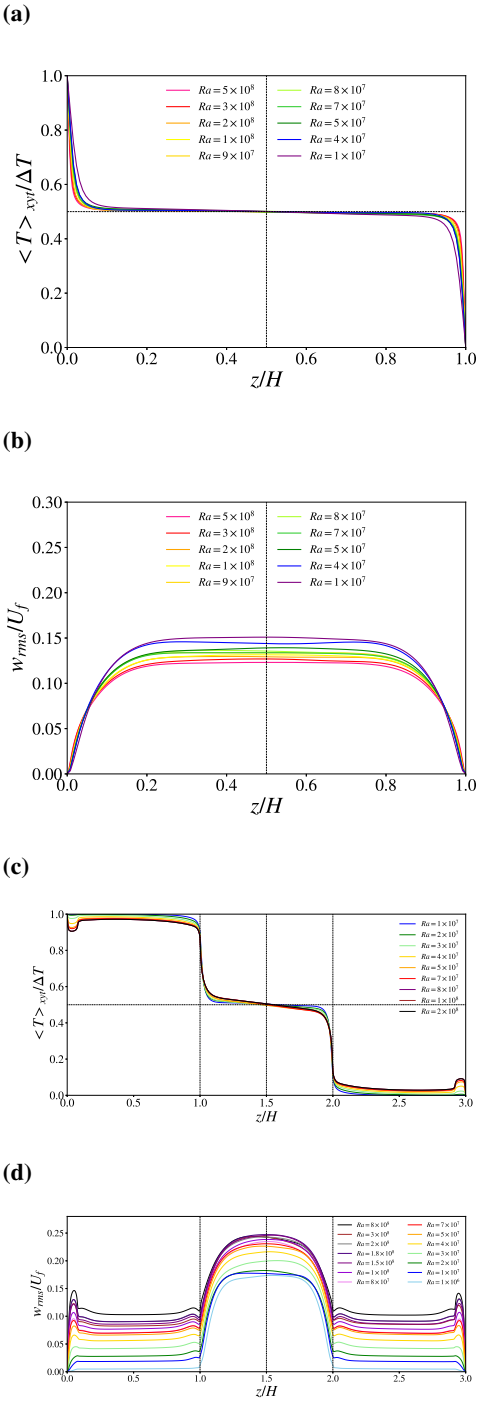

Figure 4: Mean temperature as a function of z/H for (a) conventional cases and (c) porous cases. The root-mean-square(RMS) vertical velocity normalized by U_f for (b) conventional cases and (d) porous cases. The RMS vertical velocity is defined as $w_{rms} = \langle w^2 \rangle_{xyt}^{1/2}$, in which $\langle \cdot \rangle_{xyt}$ denotes the time and horizontal averaged.

been checked in Figure 4a and Figure 4c for convectional cases and porous cases respectively. It can be seen that in the near wall region, the temperature becomes steeper and steeper in convectional cases with increasing Ra. At higher Ra, thermal boundary thickness becomes thinner. Meanwhile, for the porous cases, in the holes on the porous surfaces we have the turbulent heat flux in addition to the thermal conduction heat flux, and thus the near-wall temperature gradient does not change much.

The vertical root-mean-square velocities are shown in Figure 4b and Figure 4d for different configurations, w_{rms} in conventional cases cannot scaled with the U_f in the bulk region. In the porous cases, where a significant increase in the vertical velocity fluctuation can be observed, with respect to U_f at $Ra < 10^8$ below the ultimate regime in which the velocity fluctuation can scale with U_f. Moreover, in the porous media region($0 \leq z \leq H$ and $2H \leq z \leq 3H$), an increase w_{rms} normalized by U_f in the porous can also be observed, which may play a key role for the transition process.

Heat-flux structures, Energy dissipation and Vortical structures

The mean thickness of the thermal boundary layer is given by

$$\delta_T = -\Delta T \left(\frac{d < T >_{xyt}}{dz}\bigg|_{z=0\,or\,H} \right)^{-1} = \frac{H}{2Nu}, \qquad (10)$$

in which $z = 0$ and $z = H$ imply the non-porous cases and porous cases, respectively. The turbulent heat flux induced by the buoyancy term can describe the strength and structures of the convection. The turbulent heat flux normalized by U_f and ΔT could be obtained as $wT/(U_f \Delta T)$. It can be seen from the Figure 5 that the small scale plume structures dominate the near-wall region even at high Ra for the conventional case. However, the structures of the turbulent heat flux obtained from porous cases are so distinct and the large scale structures dominate the near-wall region, which have been observed in the ultimate state(Kawano *et al.*, 2021)).

In order to figure out the mechanism for transient behaviour towards the $1/2$ power law, the local energy dissipation rate

$$\epsilon = \frac{\nu}{2} \left(\frac{\partial u_i}{\partial x_j} + \frac{\partial u_j}{\partial x_i} \right)^2, \qquad (11)$$

is examined. In Figure 6,the horizontal and time averaged energy dissipation rate is shown as a function of z/H.

From Figure 6, we confirm that at the low Rayleigh number $Ra = 10^6$, although the weak large scale structures appear, the state in the porous media is quiescent, as represented by small energy dissipation therein. At higher Ra, the stronger large scale structures appear to enhance thermal convection as discussed before. In the transient state at $Ra < 10^8$, however, the energy dissipation in the porous media is still low with respect to U_f^3/H, the normalized dissipation there increases with increasing Ra. This less dissipation in the porous media in spite of the appearance of large scale structures enhancing thermal convection might lead to the excess of the velocity fluctuation over the buoyancy-induced terminal velocity U_f. Figure 7 shows the dependence of the local dissipation on Ra at the two positions of the porous media, $z = 0.5H$ and 0.

We see from this figure that in contrast with the above-mentioned behaviour of the local dissipation in the porous media in Figure 7a, just on the surface of the porous media in Figure 7b, the dissipation decreases with Ra at lower Ra. It is usual laminar behaviour of the normalized dissipation. At higher Ra, the dissipation in Figure 7b also increases with increasing Ra. This change of the behaviour would be attributed to the appearance of dissipative vortical structures around the porous surface. Around $Ra = 10^8$ we have enough energy dissipation in the system, so that the velocity fluctuation does not exceed U_f but scale U_f, leading to the ultimate scaling.

As the variation of the energy dissipation rate not only near the wall but also in the holes, the vortical structures' appearance, distribution and stretching can be considered as the evidences for these three states, classical, transition and ultimate. As shown in Figure 8, when the exceeded ultimate scaling $Nu \sim Ra$ occurs and continues, i.e. when the Ra is at 1×10^7 and 7×10^7, it can be seen that the energy dissipation occupies a certain distribution inside the porous medium, while the vortical structure does not enter too much, i.e. it does not provide enough dissipation for the whole system, resulting

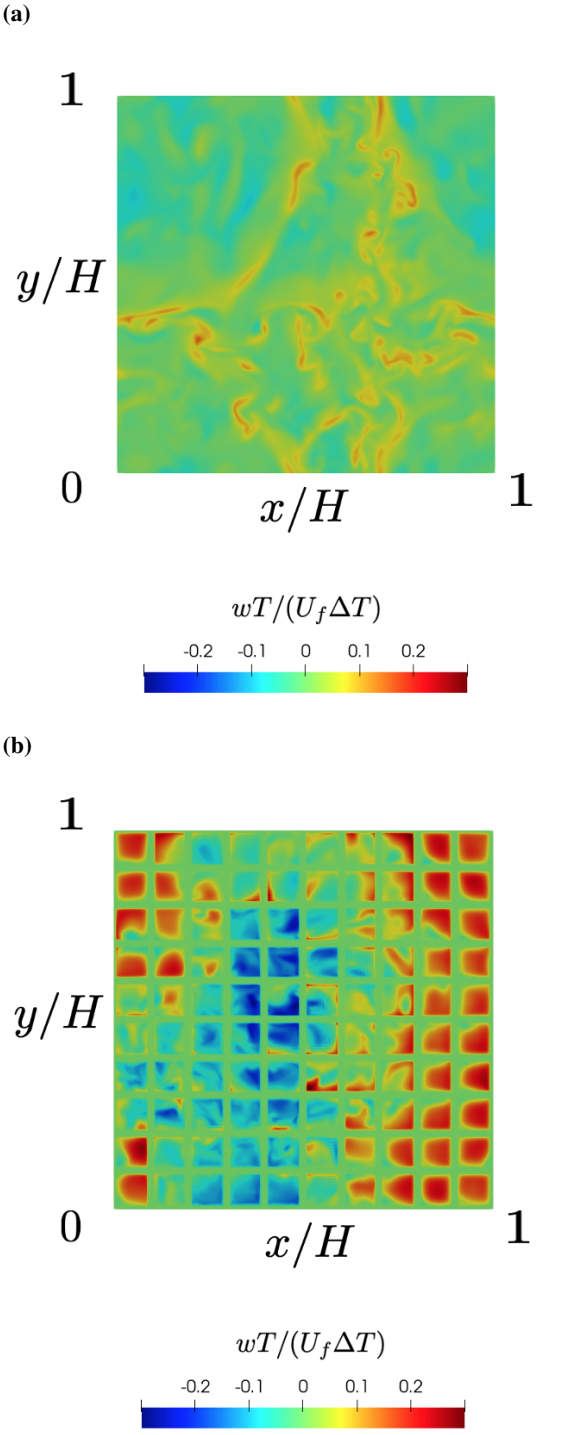

Figure 5: Turbulent heat flux wT normalized by $U_f \Delta T$ at (a) $z = 2\delta_T$ ($L_z = H$) in the non-porous case at $Ra = 5 \times 10^8$ and (b) $z - H = 5\delta_T$ ($L_z = 3H$) in the porous case at $Ra = 1.8 \times 10^8$, where δ_T denotes the thickness of a thermal conduction layer.

in an actual dissipation rate higher than the Taylor's dissipation law, $\epsilon \sim U_f^3/H$. When the Ra is at 1.8×10^8, it can be seen in Figure 8c that the smoother vortical structures start to enter the porous medium to provide sufficient energy dissipation for the system, i.e. the energy dissipation rate of whole the system will be scaled by Taylor's dissipation rate as shown in Figure 6. As the Ra increases to 8×10^8, the appearance of the energy

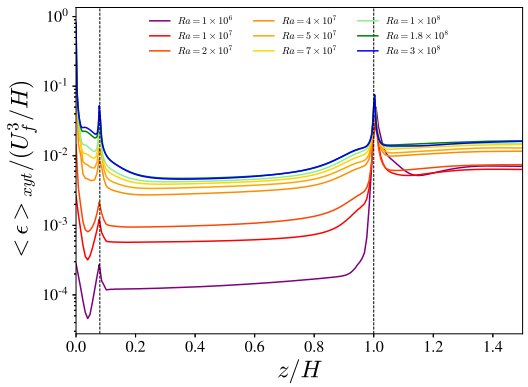

Figure 6: The horizontal and time averaged energy dissipation rate normalized by U_f^3/H in the lower half of the domain in the porous case at several values of Ra.

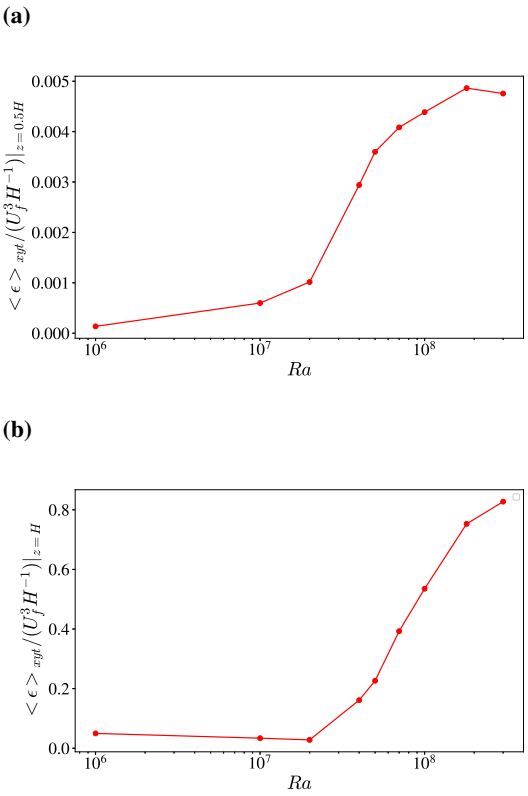

Figure 7: Local energy dissipation normalized with U_f^3/H as a function of the Rayleigh number at (a) $z = 0.5H$ and (b) $z = H$.

dissipation and vortical structures in the same time and space demonstrate that the vortical structures' stretching becomes to provide the most dissipation rate for the whole system, where the vortical structures become to be dominated within the area of the energy dissipation in the porous holes. This phenom is also consistent as the result in Figure 7, i.e. the dissipation of the whole system is in a saturated state, as the transition process to ultimate state finished.

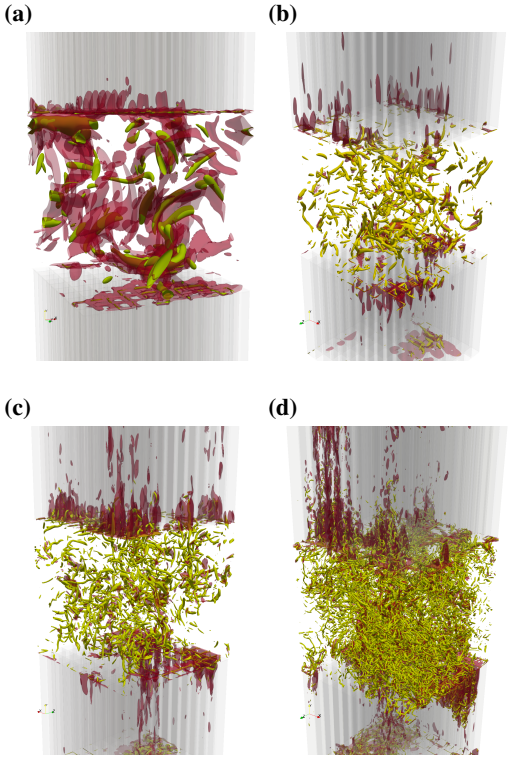

Figure 8: Instantaneous energy dissipation rate and vortical structures for porous cases at (a) $Ra = 1 \times 10^7$, (b) $Ra = 7 \times 10^7$, (c) $Ra = 1.8 \times 10^8$ and (d) $Ra = 8 \times 10^8$. The red and yellow objects, respectively, represent the isosurfaces of the energy dissipation rate and of the second invariant of the velocity gradient tensor, (a) $\epsilon/(U_f^2/H^2) = 5 \times 10$, $Q/(U_f^2/H^2) = 1.8 \times 10$, (b) $\epsilon/(U_f^2/H^2) = 1.2 \times 10^3$, $Q/(U_f^2/H^2) = 1.5 \times 10^2$, (c) $\epsilon/(U_f^2/H^2) = 1.8 \times 10^3$, $Q/(U_f^2/H^2) = 2.5 \times 10^2$ and (d) $\epsilon/(U_f^2/H^2) = 4 \times 10^3$, $Q/(U_f^2/H^2) = 5 \times 10^2$

Summary and outlook

It can clearly be observed from Figure 2, that the ultimate scaling $Nu \sim Ra^{1/2}$ is achieved by the introduction of the porous walls with chambers at high Rayleigh number $Ra \geq 10^8$. The pre-factor in the observed ultimate scaling in the case of the porous walls is roughly consistent with that found by Kawano *et al.* (2021) in the case of the permeable walls at $\beta U_f = 3$. At the lower Rayleigh number $Ra < 10^8$ in the case of the porous walls, a exceeded ultimate scaling law $Nu \sim Ra$ has been well observed and confirmed, which is so novel for this kind of research and can be recognized as the distinct results induced by the porous structures. At the much lower Rayleigh number around $Ra = 10^6$, Nu in the conventional non-porous case is almost comparable with that in the porous case, implying that the wall porosity does not have significant effects on thermal convection.

The geometry of the plume structures near the walls also shows differences between the porous cases and non-porous cases in Figure 5. It can be seen that the small-scale plume structures dominate the near-wall region even at high Ra for the conventional case. However, the structures of the turbulent heat flux found in the porous cases are so distinct, i.e, the large-scale structures dominate the near-wall region, which are essentially the same as those observed on the permeable walls

in the ultimate state (Kawano *et al.*, 2021). Meanwhile, the vertical velocity normalized by U_f not only in the bulk region but also in the near-wall region is found to be invariant in the permeable ultimate state (Kawano *et al.*, 2021), and the same is true of the porous case at high Rayleigh number $Ra > 10^8$. At the $Nu \sim Ra$ Rayleigh number $Ra = 10^7$–10^8 in the porous case, however, the vertical velocity fluctuation increases relatively to U_f.

When the porous parts are full-filled with the laminar flow, $\beta U_f \sim Ra^{1/2}$ can be achieved as the system in the state of scaling-like transition and this kind of scaling law can lead the deviant of the Nu based on the different pre-factor $c(Ra)$ in $Nu \sim c(Ra)Ra^1/2$. The variation of the pre-factor leads whole the system to enter the $Nu \sim Ra$ scaling law. As the vortical structures has been induced by the intensive turbulent structures from the bulk region, the vertical velocity in the porous and on the inter-surface between the porous part and bulk region should be well considered due to the turbulent separated vortical structures in the porous and on the near-wall region. This kind of structures could lead the vertical structures with a different scaling relationship as follows,

$$\frac{\Delta p}{\rho} \sim w^2 \sim U_f^2. \tag{12}$$

As the vortical structures enter the porous holes and try to fullfill the holes, whole the system will saturate back to the ultimate scaling from the scaling-like transition state as follows,

$$w \sim \beta \frac{\Delta p}{\rho} \tag{13}$$

$$\beta^{-1} \sim \frac{\Delta p}{\rho} w^{-1} \sim U_f. \tag{14}$$

Based on the relationship between the permeability β and U_f, $\beta U_f \sim Ra^0$ can be realized, which applies to the same configuration in (Kawano *et al.*, 2021) and the scaling law saturates back to the $Nu \sim Ra^{1/2}$ from the scaling-like transition state.

We have confirmed that at higher Ra the stronger large-scale structures appear to enhance thermal convection as discussed before. In the scaling-like transition state at $Ra = 10^7$–10^8, however, as shown in Figure 6 the energy dissipation in the porous media is still smaller than U_f^3/H, so that the normalized dissipation therein increases with increasing Ra. This less dissipation in the porous media leads to the excess of the velocity fluctuation over the buoyancy-induced terminal velocity U_f.

In this work, we have observed the ultimate state at high Rayleigh number as well as the transition with a distinct scaling law $Nu \sim Ra$ from the classical scaling to the ultimate scaling at $Ra = 10^7$–10^8 in RB convection between porous walls. We have also found that the large-scale structures become dominant even in the near-wall region for the porous cases, leading to the increase of the vertical velocity normalized by U_f. Moreover, the appearance of the large scale could be recognized as a signal of the onset of the transition process. The energy dissipation rate normalized by U_f^3/H increases with increasing Ra in the transition at low Ra, but it is invariant at high Ra, implying the Taylor's dissipation law, $\epsilon \sim U_f^3/H$. Furthermore, the relative increase in ϵ to U_f^3/H and thus the larger velocity fluctuation than U_f to enhance the energy dissipation are the mechanisms of the transitional behavior between the classical and the ultimate scaling. When the system has enough energy dissipation in the sense of the Taylor's dissipation, thermal convection is saturated down to the ultimate state.

REFERENCES

Calzavarini, E., Lohse, D., Toschi, F. & Tripiccione, R. 2005 Rayleigh and Prandtl number scaling in the bulk of Rayleigh–Bénard turbulence. *Physics of Fluids, 17* **5**, 055107.

Chavanne, X., Chilla, F., Chabaud, B., Castaing, B. & Hebral, B. 2001 Turbulent rayleigh–bénard convection in gaseous and liquid he. *Physics of Fluids, 13* **5**, 1300–1320.

Jiménez, J., Uhlmann, M., Pinelli, A. & Kawahara, G. 2001 Turbulent shear flow over active and passive porous surfaces. *Journal of Fluid Mechanics, 442* pp. 89–117.

Kawano, K., Motoki, S., Shimizu, M. & Kawahara, G. 2021 Ultimate heat transfer in 'wall-bounded' convective turbulence. *Journal of Fluid Mechanics, 914* .

Kraichnan, R. H. 1962 Turbulent thermal convection at arbitrary Prandtl number. *The Physics of Fluids* **5** (11), 1374–1389.

Laizet, S. & Lamballais, E. 2009 High-order compact schemes for incompressible flows: A simple and efficient method with quasi-spectral accuracy. *Journal of Computational Physics, 228* **16**, 5989–6015.

Laizet, S. & Li, N. 2011 Incompact3d: A powerful tool to tackle turbulence problems with up to O (105) computational cores. *International Journal for Numerical Methods in Fluids, 67* **11**, 1735–1757.

Malkus, W. V. 1954 The heat transport and spectrum of thermal turbulence. *Proceedings of the Royal Society of London. Series A. Mathematical and Physical Sciences* **225** (1161), 196–212.

Pawar, S. S. & Arakeri, J. H. 2016 Kinetic energy and scalar spectra in high Rayleigh number axially homogeneous buoyancy driven turbulence. *Physics of Fluids, 28* **6**, 065103.

Priestley, C. H. B. 1954 Convection from a large horizontal surface. *Australian Journal of Physics* **7** (1), 176–201.

Zhu, X., Stevens, R. J., Shishkina, O., Verzicco, R. & Lohse, D. 2019 Scaling enabled by multiscale wall roughness in Rayleigh–Bénard turbulence. *Journal of Fluid Mechanics, 869* .